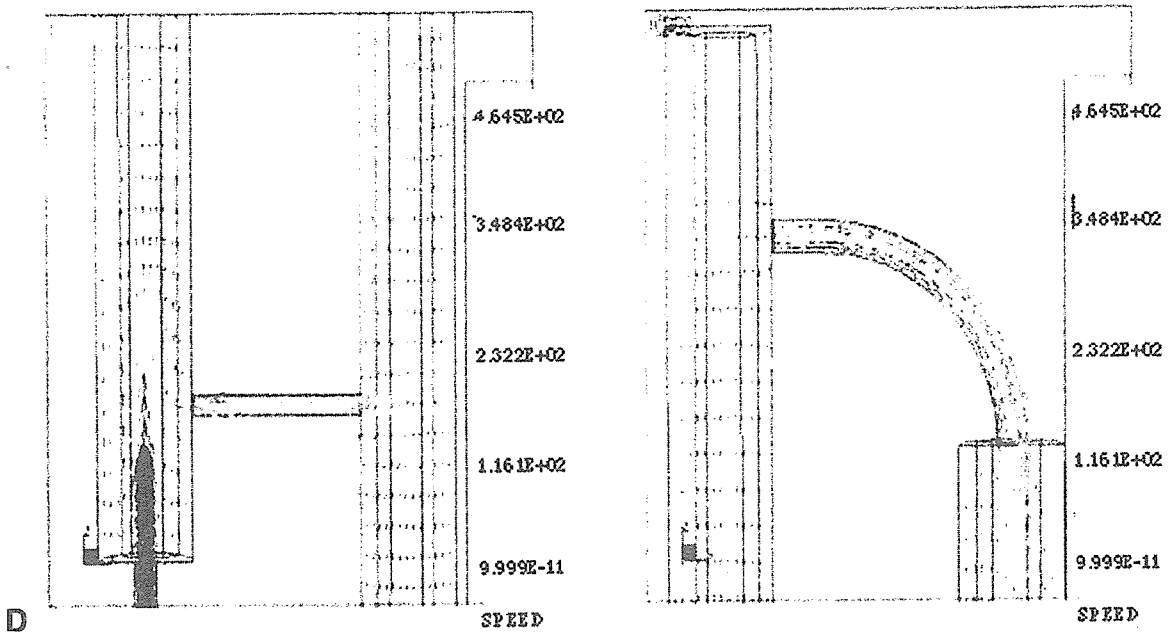

Figure 1D.

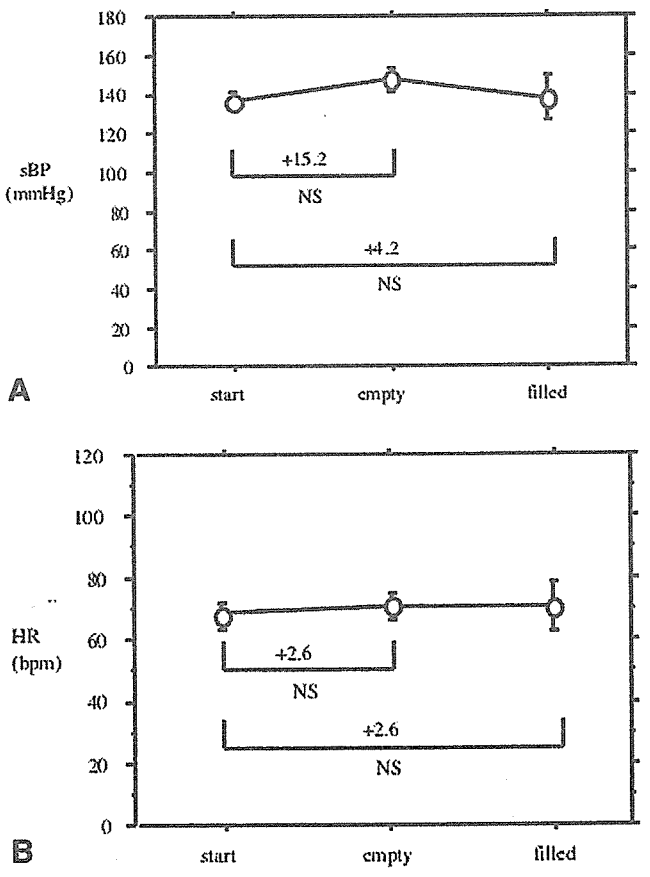

Figure 2. a: Induction of hypotension by starting hemodialysis. Measurement of systolic blood pressure (sBP): start = immediately before start of hemodialysis; empty = 10 minutes after start of hemodialysis; filled = 20 minutes after start of hemodialysis. **b:** Induction of hypotension by starting hemodialysis. Measurement of heart rate (HR): start = immediately before start of hemodialysis; empty = 10 minutes after start of hemodialysis; filled = 20 minutes after start of hemodialysis.

a small amount of blood clotted in the dialyzer. However, during the next dialysis session when the amount of heparin was increased 1.5 times, blood clots did not form in the chamber. Blood clot formation in the circuit was not observed in the other patients during usual dialysis or C-C dialysis.

Risk of Pushing a Portion of the Blood Volume Back Into the Dialyzer

At the time of discharge, there is a potentially serious risk of pushing a portion of the blood volume back into the dialyzer and not into the patient; however, there was no change in transmembrane pressure and venous pressure, so there was no machine alarm.

Discussion

Influence of Increased Priming Volume

To increase intracorporeal BV during hypotension, we made it possible to change the volume in the chamber in the venous line of the extracorporeal circulation circuit. As a result, compared with the priming volume of the usual extracorporeal circulation circuit (70–170 ml), volume increased slightly to 172 ml. However, neither a significant decrease in BP nor an increase in HR at the initiation of the extracorporeal circulation was induced.

Influence of Chamber Structure Complexity

The chamber structure becomes more complex with the added ability to change the volume in the venous chamber; therefore, blood clot formation in the chamber becomes a concern. Results showed that distinguishable clot formation was not noted in C-C except for one patient who had a tendency to form blood clots in the circuit even during usual dialysis. Distinguishable clot formation was not observed by increasing the amount of anticoagulant, thus, it seemed that if

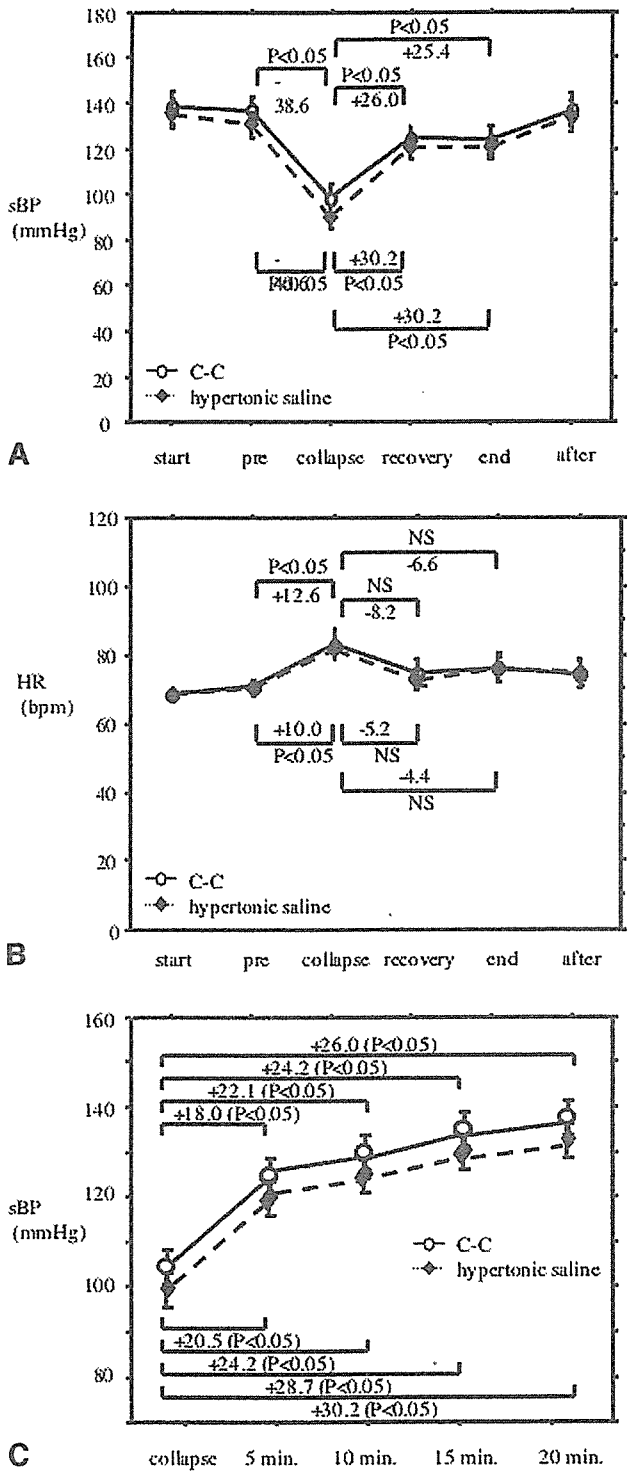

Figure 3. a: Effect on blood pressure (BP) recovery from hemodialysis (HD) collapse. Measurement of systolic blood pressure (sBP): start = immediately before start of dialysis; Pre = 30 minutes before hemodialysis collapse occurred; recovery = 20 minutes after blood administration from the charging-chamber (C-C); end = immediately before the end of dialysis; after = 20 minutes after the end of dialysis. **b:** Effect on blood pressure (BP) recovery from hemodialysis collapse. Measurement of heart rate (HR): start = immediately before start of dialysis; Pre = 30 minutes before hemodialysis collapse occurred; recovery = 20 minutes after blood administration from the charging-chamber (C-C); end = immediately before the end of dialysis; after = 20 minutes after the end of dialysis. **c:** Measurement of sBP at hemodialysis collapse. 5, 10, 15, 20 min. = 5, 10, 15, and 20 minutes after hemodialysis collapse.

Table 2. Dialysis Conditions under the C-C and Hypertonic Saline Methods for Treatment of Hemodialysis Collapse

Dialysis Condition	Charging Chamber	Hypertonic Saline
Weight gain (kg)	2.14 (0.62)	2.11 (0.62)
Water deletion speed (ml/h)	589.1 (174.0)	591.4 (198.7)
Collapse time (min)	182.5 (43.2)	178.5 (36.2)
Total hemodialysis time (min)	228.5 (39.7)	226.0 (39.3)

Values are mean (standard deviation).

clot formation in the circuit was not observed during usual dialysis, it would not be observed during dialysis using C-C.

Effect of BP Recovery

The 10% NaCl solution has hypertonic osmolality and increases effective circulating blood volume temporarily, so it has been reported that hypertonic saline is effective for hemodialysis collapse.[11] This study has proven that using C-C attains almost the same effect of BP recovery as the intravenous administration of 20 ml 10% NaCl. With this method, BP recovery is possible without the need for injection of additional solutions. Therefore, it is a useful method that has the added advantage of reducing medical costs.

Future Implications

It is possible to reduce priming volume by reducing the volume of the arterial chamber or the inner diameter of the blood circulation circuit. With the current circuit, hypotension did not occur during blood withdrawal at the beginning of dialysis; however, the risk can be reduced further by any decrease in the priming volume.

The most complicated technique in the dialysis method using C-C is to manually withdraw any air from the venous chamber or to return blood into the body rapidly. The speed of the operation and the adjustment of the volume are dependent on the operator's manual skill at present. The development of a device that automatically withdraws air from

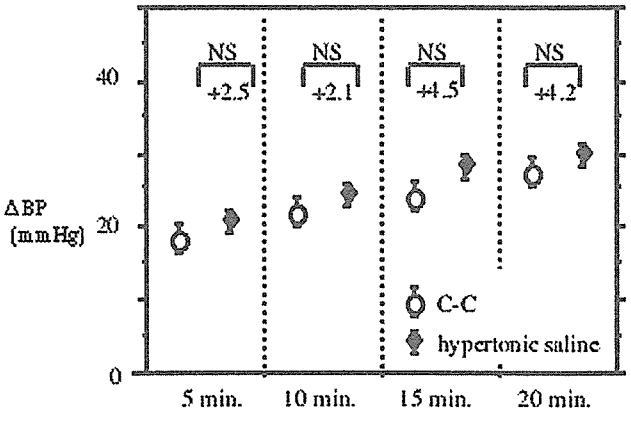

Figure 4. Comparison of BP recovery effect. There were no significant differences in total amount of fluid, total hemodialysis time, and BP recovery effect at 5, 10, 15, and 20 minutes (p = 0.5346, 0.8315, 0.6342, 0.4196, respectively). The BP recovery effect in both groups (ΔBP) was calculated as recovery systolic BP minus collapse systolic BP.

the chamber and administers blood volume as needed is under investigation. This blood charging and discharging is available only one time, so it is not available for patients with repeated hypotension during a single dialysis session.

Blood clot formation in the chamber should be fully considered, and it is necessary to examine the increase in anticoagulant according to the need.

Conclusion

Until now, infusion has been performed to increase BV for hemodialysis collapse. Our study proved that BP recovery is possible by returning blood from the chamber directly into the body using a charging chamber for hemodialysis collapse. The concept of the charging chamber is new and has an economical advantage, because dialysis can be resumed without infusion. Also, additional water deletion for the volume of infusion is not needed, so the efficiency of the dialysis session increases. If hypertonic saline is used, thirst appears frequently and angiopathic change may occur. Therefore, dialysis using C-C seems to be an effective method for treatment of hemodialysis collapse.

References

1. Henrich WL: Hemodynamic instability during hemodialysis. *Kidney Int* 30: 605–612, 1986.
2. Converse RL Jr, Jacosen TN, Jost CM *et al*: Paradoxycal withdrawal of reflex vasoconstriction as a cause of hemodialysis-induced hypotension. *J Clin Invest* 90: 1657–1665, 1992.
3. Yokokawa K, Mankus R, Saklayen MC *et al*: Increased nitric oxide production in patient with hypotension during hemodialysis. *Ann Intern Med* 123: 35–37, 1995.
4. Shinzato T, Miwa M, Nakai S *et al*: Role of adenosine in dialysis induced hypotension. *J Am Soc Nephrol* 4: 1987–1994, 1994.
5. Levy FL, Grayburn PA, Foulks CJ, *et al*: Improved left ventricular contractility with cool temperature hemodialysis. *Kidney Int* 41: 961–965, 1992.
6. Jamil KM, Yokoyama K, Takemoto F, *et al*: Low temperature hemodialysis prevents hypotensive episodes by reducing nitric oxide synthesis. *Nephron* 84: 284–286, 2000.
7. Sang GL, Kovithovongs C, Unan R, Kjellstrand CM: Sodium ramping in hemodialysis: A study of beneficial and adverse effects. *Am J Kidney Dial* 29: 669–677, 1997.
8. Wolkotte C, Hassell DR, Moret K, *et al*: Blood volume control by biofeedback and dialysis-induced symptomatology: A short-term clinical study. *Nephron* 92: 605–9, 2002.
9. Splendiani G, Costanzi S, Passalacqua S, *et al*: Sodium and fluid modulation in dialysis: New approach. *Nephron* 89: 377–380, 2001.
10. Cai Y, Zimmerman A, Ladefoged S, Secher NH: Can haemodialysis-induced hypotension be predicted? *Nephron* 92: 582–588, 2002.
11. Gong R, Lindberg J, Abrams J, *et al*: Comparison of hypertonic saline solutions and dextran in dialysis-induced hypotension. *J Am Soc Nephrol* 3: 1808–1812, 1993.
12. van der Sande FM, Kooman JP, Barendregt JN, *et al*: Effect of intravenous saline, albumin, or hydroxyethylstarch on blood volume during combined ultrafiltration and hemodialysis. *J Am Soc Nephrol* 10: 1303–1308, 1999.
13. Van der Sande FM, Luik AJ, Kooman JP, *et al*: Effect of intravenous fluids on blood pressure course during hemodialysis in hypotensive-prone patients. *J Am Soc Nephrol* 11: 550–555, 2000.
14. Shimoyama H, Suwata J, Saitoh H, *et al*: Changes in catecholamine level in hypotensive patients subjected to dialysis. *Nippon Jinzo Gakkai Shi* 31: 165–170, 1989.
15. Flynn JJ 3rd, Mitchell MC, Caruso FS, Mcelligott MA: Midodrine treatment for patients with hemodialysis hypotension. *Clin Nephrol* 45: 261–267, 1996.
16. Lim PS, Yang CC, Li HP, *et al*: Midodrine for the treatment of intradialytic hypotension. *Nephron* 77: 279–283, 1997.
17. Pang CC: Autonomic control of the venous system in health and disease: effects of drugs. *Pharmacol Ther* 90: 179–230, 2001.
18. Pitts RF: *Physiology of the Kidney and Body Fluids*. Chicago, Year Book Medical Publishers, 1974, pp. 20-41.

Reprinted from
J Arrhythmia Vol 22 No 1 2006

Original Article

Conduction Velocity around the Tricuspid Valve Annulus during Typical Atrial Flutter by Electro-anatomic Mapping System

Akira Sawa MD, Akihiko Shimizu MD, Takeshi Ueyama MD, Yasuhiro Yoshiga MD, Shinsuke Suzuki MD, Naoki Sugi MD, Masunori Matsuaki MD

Department of Cardiovascular Medicine, Yamaguchi University Graduate School of Medicine

Original Article

Conduction Velocity around the Tricuspid Valve Annulus during Typical Atrial Flutter by Electro-anatomic Mapping System

Akira Sawa MD, Akihiko Shimizu MD, Takeshi Ueyama MD, Yasuhiro Yoshiga MD, Shinsuke Suzuki MD, Naoki Sugi MD, Masunori Matsuaki MD

Department of Cardiovascular Medicine, Yamaguchi University Graduate School of Medicine

Objective: Conduction velocity around the tricuspid valve annulus (TA) during typical atrial flutter (AFL) has been shown to be slowest in the inferior vena cava-tricuspid valve (IVC-TV) isthmus when compared to the septal or free wall segments of the TA. We investigated the conduction velocity in IVC-TV isthmus, dividing into three areas. Methods: We evaluated conduction velocity around the TA during typical AFL in 10 patients, using an electro-anatomic mapping system (CARTO™). Conduction velocity was calculated at six areas around the TA including the septal wall, upper wall, lateral wall, and isthmus wall, which was further divided into three areas, lateral isthmus, mid isthmus, and septal isthmus. Results: Conduction velocity around the TA during typical AFL was slowest in the IVC-TV isthmus. Further, conduction velocities (m/sec) in the mid isthmus (0.44 ± 0.17) and septal isthmus (0.45 ± 0.22) were significantly slower ($p < 0.05$) than that in the upper wall (0.67 ± 0.26). Conclusions: The relatively slower conduction in IVC-TV isthmus resulted from the relatively slower conduction in the area from mid to septal isthmus.
(J Arrhythmia 2006; 22: 31–36)

Key words: Conduction velocity, Atrial flutter, Electro-anatomic mapping system

Introduction

Atrial flutter (AFL) has been defined traditionally as an atrial-tachycardia with a rate above 240 bpm and a continuously waving baseline. However, electrophysiologic studies (EPS) have put in evidence the inadequacy of current classifications of atrial tachycardias and AFL, based only the ECG pattern.[1] The orifices of the superior vena cava (SVC) and inferior vena cava (IVC), linked by the Crista terminalis thus constitute the posterior obstacle and the Tricuspid Annulus (TA), the anterior obstacle that make the virtual ring of myocardium supporting reentry in typical AFL.[2] Typical AFL activation turns in a ring of muscle bounded anterior by the TA and posterior by the openings of both vena cavae and the line of functional block in the posterior wall of the right atrium (RA). The IVC-TV isthmus (CTI) is an essential part of the typical AFL circuit, and the isthmus has been identified as an area of the slow conduction.[3–6]

Some authors have already found that conduction

Received 10, October, 2005: accepted in final form 23, January, 2006.
Address for correspondence: Akira Sawa MD, Department of Cardiovascular Medicine, Yamaguchi University Graduate School of Medicine 1-1-1 Minami-kogushi, Ube, Yamaguchi, Japan 755-8505. TEL: 0836-22-2248 FAX: 0836-22-2246
E-mail: firstrebirth@yahoo.co.jp

through the isthmus was slower than that though the anterior RA wall.[7] But activation of the low RA usually covers less than 30% of the cycle, far from the 70–80% in ventricular tachycardia (VT), and conduction is modestly slower and fragmented electrograms are not present before radiofrequency application. Up to now, the multi-polar catheter, for example the HALO 20-pole catheter, had been used to identify AFL activation around the TA. A better understanding of the electrophysiologic substrate of typical AFL is of scientific interest, particularly the precise location of the area of slow conduction in the reentrant circuit.

In recent years electro-anatomic mapping systems have come to be used frequently for EPS, and it is useful for the identification of a complex tachyarrhythmia circuit. One such system, the CARTO electro-anatomic mapping system, produces a three dimensional, high-resolution anatomic activation map of the entire AFL circuit in the right atrium.[8–10] Electro-anatomic mapping systems allow the distance and the time difference can be measured, and thus the conduction velocity can be calculated.

In the present study, we investigated the conduction velocity around the TA in typical AFL patients, especially focusing in greater detail on the isthmus, using the electro-anatomic mapping system.

Methods

1) Patients characteristics

The study population consisted of 10 patients (7 men and 3 women, age 57 ± 13 years) with typical atrial flutter ECG (**Table 1**). By electro-cardiographic criteria, atrial flutter was classical in appearance (saw-toothed pattern in inferior leads) in all patients. They were referred for radiofrequency catheter ablation (RFCA). Five patients had a history of paradoxical atrial fibrillation. Six patients had cardiovascular diseases, including four with hypertension, one with valvular disease and one with coronary disease.

2) Electrophysiologic study

Informed written consent was obtained from all patients. As described previously, all anti-arrhythmia drugs were discontinued for at least five half-lives before the study.[11] In all patients, a 7-French 20-pole, deflectable Halo catheter with 10-mm paired spacing was positioned around the TA to record RA activation in the high septal wall, roof, lateral wall, and CTI simultaneously. A 5-French, deflectable, 10-pole catheter with 2-mm interelectrode distance and 5-mm space between each electrode pair also was inserted into the coronary sinus via the subclavian vein. The position of the proximal electrode pair was at the ostium of the coronary sinus. 5-french multi-polar catheters were placed at high right atrium, His bundle, and right ventricular apex. A 8-French sheath (Preface Biosense-Webster, Johnson & Johnson, USA) placed in the right femoral vein was used to introduce the electro-anatomic mapping catheter. A 7-French, 4-mm tip electrode mapping/ablation catheter (NAVI-STAR Biosense-Webster, Johnson & Johnson, USA) was advanced into the right atrium. Three-dimensional atrial mapping was started in sinus rhythm in most of the patients. If spontaneous AFL was found at the onset of the study, Halo catheter mapping, and electro-anatomic mapping were performed to investigate the reentrant circuit. When the study found the presence of typical AFL mapping was performed during the AFL. If sinus rhythm was present at baseline, low RA or coronary sinus pacing until 2:1 atrial capture was preformed to induce AFL. When AFL was induced a new map was started, initially using the anatomical information obtained during sinus rhythm. Then, the right atrial geometry was rewritten at a different point from that during sinus rhythm. All stimuli were delivered through an external stimulator at a 2-msec pulse width at twice the diastolic threshold.

3) Electroanatomic mapping system

The CARTO™ nonfluoroscopic electro-anatomic mapping and navigation system (Biosense-Webster, Johnson & Johnson, USA) has been recently described elsewhere. A 4-mm tip catheter (NAVI-STAR,

Table 1 Clinical characteristics of patients.

Pt	Age (year)	Sex (M/F)	Diagnosis (Excluding AFL)	AFLCL (msec)
1	54	M	Coronary disease, HT	245
2	74	M	PAF, HT	290
3	76	M	None	285
4	70	M	None	270
5	55	M	PAF, Valvular disease	255
6	52	M	HT	285
7	54	M	PAF, HT	235
8	48	F	LV dysfunction	340
9	59	F	PAF	250
10	31	F	PAF	240
Mean ± SD	57 ± 13			269 ± 32

AFL = atrial flutter, PAF = paroxysmal atrial fibrillation, HT = hypertension, LV = Left ventricular, AFLCL = atrial flutter cycle length.

Biosense-Webster, Johnson & Johnson, USA) was used for the mapping and ablation. Because of its positional and morphological stability, the electrogram recorded by the coronary sinus catheter was chosen to be the reference for local activation time. The three-dimensional geometry of the chamber is reconstructed in real time with electrophysiologic information, which is color coded and superimposed on the anatomic map. The right atrium was plotted by dragging the mapping catheter over the endocardium. Mapping was complete when all lesions of the right atrium had been systematically sampled and when a sufficient density of points had been acquired to determine the circuit during AFL.

4) Catheter ablation

RFCA of the CTI was performed by using with a 4-mm tip catheter (NAVI-STAR, Biosense-Webster, Johnson & Johnson, USA) during AFL or pacing from the proximal coronary sinus during sinus rhythm.

The preset temperature was 55–60 degrees and the preset duration of each RF was 60 seconds. RFCA application was performed to create linear lesions in the CTI. Successful ablation was defined as achievement of bidirectional isthmus and gap conduction block without induction of typical AFL.

5) Definitions

Typical AFL was defined as a macro-reentrant atrial tachycardia circulating around the TA and using the CTI. Counter-clockwise (CCW) typical AFL was defined as a typical atrial flutter with a descending activation sequence in the free wall and an ascending sequence in the septal wall. Clockwise (CW) typical AFL was defined as a typical atrial flutter with a descending activation sequence in the septal wall and an ascending sequence in the free wall. Scar area was defined from an electrophysiological standpoint as an electrically silent area with an EGM amplitude of <0.04 mV that displays no distinguishable or repetitive EGM patterns.

6) Management after ablation and follow up

After ablation patients were monitored for 48 hours by telemetry. Transthoracic echocardiography was preformed by the end of the same day after ablation.

7) Measurement

The RA, based on the anatomical map, was observed from the left anterior oblique projection, and the screen was set so that the TA might come to the front only in the side of rotation. A perpendicular line initially was dropped from the picture, then two lines that intersected this line by 45 degrees were set (**Figure 1a**).

The area surrounding the TA was divided into four with borders at these two orthogonal lines. These divided areas were defined as the following. The one

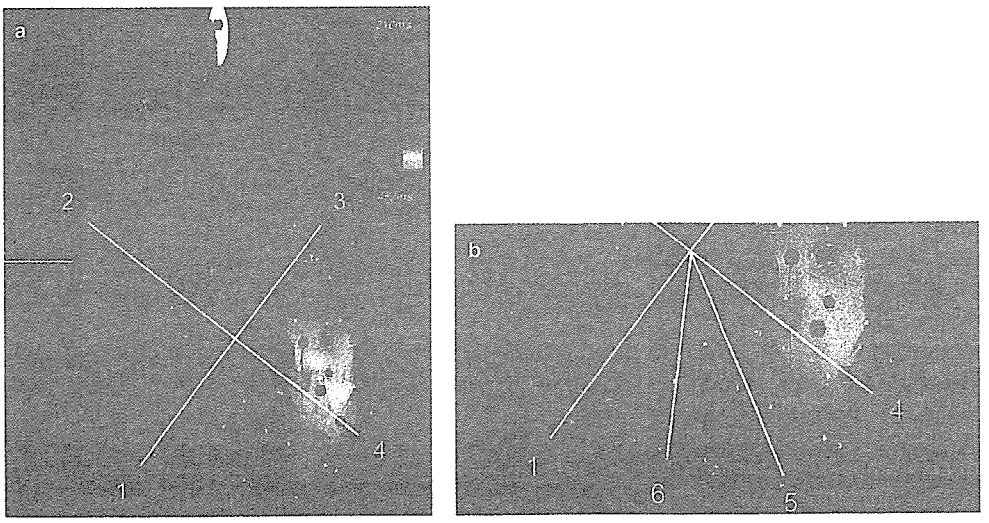

Figure 1

a: Right atrium was observed from the left anterior oblique projection, the screen was set so that the TA might come to the front only in the side of rotation. The 4 areas surrounding on the TA was divided into four bordering these two orthogonal lines, and these were defined as lateral wall (1-2), upper wall (2-3), septal wall (3-4), and isthmus (4-1).

b: The isthmus area was divided into three computation areas by equiangular degrees, and these were defined as septal isthmus (4-5), mid isthmus (5-6), and lateral isthmus (6-1).

including the CTI (anatomical isthmus) was defined as the isthmus area, and from there in a clockwise direction as lateral wall, upper wall, and septal wall. The percentage of conduction time in the area of isthmus to the cycle length of AFL was calculated. The isthmus area was divided into three computation areas, and these were defined as septal isthmus, mid isthmus, and lateral isthmus (**Figure 1b**). These six areas around the TA were set as stated above. The pattern of the excitement conduction was confirmed in the activation map. Two adjoining points (separated by a distance of 5 mm to 20 mm) were set to the vicinity of the center in these areas within 15 mm from the TA ring and the two points were set at the direction of the line between two points as parallel as possible to the TA ring.

8) Distance and conduction velocity measurement

Conduction velocity was calculated as the ratio of the distance between the two points and the difference in activation time between these two points.

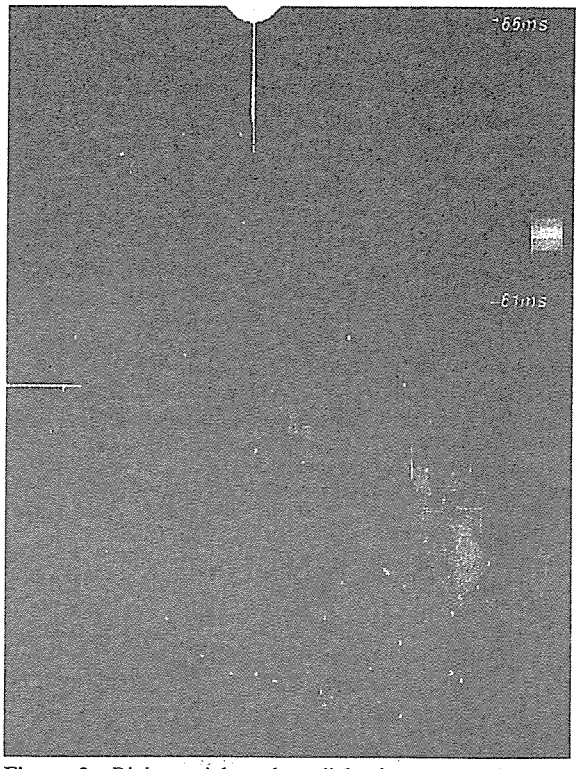

Figure 2 Right atrial endocardial electroanatomic map (Isochronal map: isochronal step = 10 msec) in a patient (#4) with typical AFL.
Note the counterclockwise flutter activation sequence around the tricuspid annulus, indicating the common or typical form of type1 AFL. The colors represent early (red) to late (purple) activation, referenced to the proximal coronary sinus electrode. Red dots indicate ablation points.

This distance of two points was assumed to be 20 mm from 5 mm this time (<5 mm, to minimize the error caused by endocardial curvature).

9) Statistical analysis

Continuous values are expressed as mean ± standard deviation. One-way analysis of variance (ANOVA) with Bonferoni–Dunn method for pair multiple comparisons was used to determine the statistical significance of the difference in mean values for conduction velocity between the various areas around the TA. A P-value of 0.05 or less was considered significant.

Results

1) Mapping results

In the all 10 patients, complete electro-anatomic maps were obtained for typical AFL (mean cycle length = 269 ± 32 msec, range 220–340 msec). All patients had CCW activation of RA limited anteriorly by the TA, an example of which is shown in **Figure 2**. Pacing from the CTI during atrial flutter showed concealed entrainment with the post-pacing-interval equal to flutter cycle length in all patients. During CCW atrial flutter, the leading edge of the activation wavefront emerged from the low postero-septal region, traveled up the septal and posterior wall, reached the roof, spread down the antero-lateral wall, and entered the CTI. The direction of the activation wavefront demonstrated by electro-anatomic mapping system was consistent with the activation sequence recorded by the HALO catheter in all patients. The percentage of conduction time in the area of isthmus to the cycle length of AFL (269 ± 32 msec) was 34 ± 5%.

2) Analysis of regional conduction velocities

In all patients, the conduction velocities in the six areas were measured. Regarding the distance of the two points in these six areas, the longest distance was observed in the septal wall, followed by the upper wall, lateral wall, lateral isthmus, and septal isthmus, while the nearest distance was found in the mid isthmus (12.5 ± 6.3 mm, 11.9 ± 4.1 mm, 10.3 ± 3.6 mm, 9.6 ± 4.3 mm, 8.8 ± 3.7 mm and 8.0 ± 4.5 mm; N.S), no significant difference was seen in these six areas. Of the six areas around TA initially analyzed (**Table 2**), mean conduction velocity (m/sec) was significantly slower ($p < 0.05$) in the mid isthmus (0.44 ± 0.17) and septal isthmus (0.45 ± 0.22), than in the upper wall (0.67 ± 0.26). Mean conduction velocity tended to be slow ($p = 0.06$) in the mid isthmus and septal isthmus compared with

Table 2 Conduction velocity (m/sec) in 6 areas around the TA during AFL.

Pt	Septal wall	Upper wall	Lateral wall	CTI		
				Lateral	Mid	Septal
1	0.37	0.35	0.58	0.35	0.30	0.26
2	0.88	0.53	0.80	0.38	0.51	0.29
3	1.00	0.58	0.72	0.62	0.58	0.69
4	0.40	1.11	0.58	0.60	0.35	0.72
5	0.86	0.48	0.54	0.99	0.27	0.50
6	0.64	0.50	0.66	0.51	0.47	0.49
7	0.32	0.59	0.49	0.30	0.51	0.73
8	0.44	0.61	0.46	0.92	0.66	0.13
9	0.64	1.09	0.51	0.43	0.64	0.42
10	0.57	0.86	0.93	0.62	0.14	0.23
Mean ± SD	0.61 ± 0.24	0.67 ± 0.26	0.63 ± 0.15	0.57 ± 0.23	0.44 ± 0.17*#	0.45 ± 0.22*#

Septal wall = right atrial septal wall, upper wall = right atrial upper wall, lateral wall = right atrial lateral wall, CTI = IVC-TV isthmus, lateral = lateral isthmus, mid = mid isthmus, septal = septal isthmus.
* = $P < 0.05$ comparing mid isthmus and septal isthmus to upper wall.
# = $P = 0.06$ comparing conduction velocity in all other segments.

all other segments. In these patients, lowest conduction velocities in each case were in isthmus area (5 patients in mid isthmus, 4 patients in septal isthmus, 1 patient in lateral isthmus).

Discussion

This study has shown that the medial mid-isthmus and septal isthmus are the slowest-conducting areas in the reentrant circuit in typical AFL in humans. Although the patient numbers studied were small, and therefore this cannot be substantiated by this study, it is consistent with previous studies. Previous studies, the earliest of which used pacing entrainment and multi-electrode catheter mapping technique, have consistently demonstrated that the TV-IVC isthmus is an area of slow conduction in the AFL reentrant circuit.[12,13]

Tai et al. measured isthmus conduction velocity during pacing (but not AFL) by dividing the bipolar electrogram intervals by interelectrode spacing and found that isthmus conduction velocities were lower than in our study (0.336 ± 0.045 m/sec) and were lower in the mid isthmus compared with the lateral isthmus.[14] This may be explained because distance traveled across a complex curved surface is likely to underestimated the distance between electrodes on a straight catheter bridging this distance. Shilling et al. measured isthmus conduction velocity during AFL by noncontact mapping system (Ensite™) and found that isthmus conduction velocities were higher than in our study (0.74 ± 0.36 m/sec).[15]

Hassankhani et al. measured conduction velocity during AFL around the TA by electro-anatomic mapping system (CARTO™) and found that inferior septum and medial isthmus were the areas of slowest conduction in typical AFL,[16] which findings were similar to our results.

In isolated pig and dog hearts, Hocini et al. reported that fibers were parallel to the TA in the posterior part of Triangle-of-Koch. In the midjunctional area, the direction of the fibers changed to an orientation perpendicular to the TA. During stimulation from posterior and anterior sites, activation proceeded parallel to the TA at a high conduction velocity (0.5 to 0.6 m/sec). During stimulation from sites near the coronary sinus, a narrow zone of slow conduction occurred in the posterior part of the Triangle-of-Koch where activation proceeded perpendicular to the fiber orientation. Above and below this zone, conduction was fast and parallel to the annulus.[17] A correlation was observed between parallel versus perpendicular fiber orientation with respect to the TA and fast versus slow conduction in the triangle-of-Koch. These observations of myocardial fiber anisotropy in the triangle-of-Koch[17–19] are consistent with the observations from this study and may account for the fact that the slowest conduction in the AFL circuit is in areas of the septal isthmus.

In this study, typical AFL with relatively slower conduction in IVC-TV isthmus resulted from the relatively slower conduction in the area from mid to septal isthmus. This relatively slower conduction area is supposed be related to the onset and

maintenance of AFL. However, further examination will be necessary to prove this issue.

Study Limitation

In measuring conduction velocity distance, measurements were calculated using a series of short straight-line distance that an approximation of the true curved surface of the RA and are therefore subject to error. The closer the distance between two points, the less error is introduced in calculating the distance between two points on a sphere, given that a line is the asymptotic measure of two points with closest proximity on a curved surface. It is enumerated that neither the direction where the wave side travels nor the set direction of these two points are completely corresponding.

Conclusion

Electroanatomic mapping system of the right atrium in patients with typical AFL reveals that the relatively slower conduction in IVC-TV isthmus resulted from relatively slower conduction in the area from the mid to septal isthmus, and the mid isthmus is the region of slowest conduction around the TA.

References

1) Saoudi N, Cosio F, Waldo A, Ches S-A, Iesaka Y, Lesh M, Saksena S, Salermo J, Schoels W: Classification of atrial flutter and regular atrial tachycardia according to electrophysiologic mechanism and anatomic basis: A statement from a joint expert group from the working group of arrhythmias of European Society of Cardiology and the North American Society of Pacing and Electrophysiology. J Cardiovasc Electrophysiol 2001; 12: 852–866
2) Cosio FG, Arribas F, Lopez Gil M, Palacios J: Atrial flutter mapping and ablation. I. Studying atrial flutter flutter mechanisms by mapping and entrainment. PACE 1996; 19: 841–853
3) Waldo AL: Pathogenesis of atrial flutter. J Cardiovasc Electrophysiol 1998; 9: S18–25
4) Daoud EG, Morady F: Pathophysiology of atrial flutter. Annu Rev Med 1998; 49: 77–83
5) Disertori M, Inama G, Vergara G, Guarnerio M, Del Favero A, Fulanello F: Evidence of a reentry circuit in the common type of atrial flutter in man. Circulation 1983; 67: 434–440
6) Chauchemez B, Haissaguerre M, Fisher B, Thomas O, Clementy J, Coumel P: Electrophysiological effects of catheter ablation of inferior vena cava-tricuspid annulus isthmus in common atrial flutter. Circulation 1996; 93: 284–294
7) Tai C-T, Chen S-A, Chiang C-E, Lee S-H, Ueng K-C, Wen Z-C, Huang J-L, Chen Y-J, Yu W-C, Feng A-N, Chiou C-W, Chang M-S: Characterization of low right atrial isthmus as the slow conduction zone and pharmacological target in typical atrial flutter. Circulation 1997; 96: 2601–2611
8) Nakagawa H, Jackman WM: Use of a three-demensional, nonfluoroscopic mapping system for catheter ablation of typical atrial flutter. Pacing Clin Electrophysiol 1998; 21: 1279–1286
9) Feld GK: Evolution of diagnostic and interventional cardiac electrophysiology: A brief historical review. Am J Cardiol 1999; 84: 115R–124R
10) Gepstein L, Hayam G, Benttaim SA: A novel method for non fluoroscopic catheter-based electroanatomical mapping of the heart: In vitro and vivo accuracy results. Circulation 1997; 95: 1611–1622
11) Kakugawa H, Shimizu A, Yamagata T, Esato M, Ueyama T, Yoshiga Y, Kanemoto M, Matsuzaki M: Decrease in the spatial dispersion at the termination of atrial fibrillation by intravenous cibenzoline. Circ J 2003; 67: 810–815
12) Feld GK, Mollerus M, Brigersdotter-Green U, Fujimura O, Bahnson T, Boyce K, Rahme M: Conduction velocity in the tricuspid valvu-inferior vena cava isthmus is slower in patients with typel atrial flutter compared to those without a history of atrial flutter. J Cardiovasc Electrophysiol 1997; 8: 1338–1348
13) Shah DC, Jais P, Haissaguerre M, Chouairi S, Takahashi A, Hocini M, Garrigue S, Clementy J: Three-dimensional mapping of the common atrial flutter circuit in the right atrium. Circulation 1997; 96: 3904–3912
14) Tai C, Chen S, Chiang C, Lee S, Ueng K, Wen Z, Huang J, Chen Y, Yu W, Feng A, Chiou C, Chang M: Characterization of low right atrial isthmus as the slow conduction zone and pharmacological target in typical atrial flutter. Circulation 1997; 96: 2601–2611
15) Shilling RJ, Peters NS, Goldberger J, Kadish AH, Davies DW: Characterization of the anatomy and conduction velocities of the human right atrial flutter circuit determined by noncontact mapping. J Am Coll Cardiol 2001; 38: 385–393
16) Hassankhani A, Yao B, Feld GK: Conduction velocity around the tricuspid valve annulus during type 1 atrial flutter: Defining the location of areas of slow conduction by three-dimensional electroanatomical mapping. J Interv Card Electrophysiol 2003; 8: 121–127
17) Hocini M, Loh P, Ho SY, Sanches-Quintana D, Thibault B, de Bakker JM, Janse MJ: Anisotropic conduction in the triangle of Koch of mammalian hearts: Electrophysiologic and anatomic correlations. J Am Coll Cardiol 1998; 31: 629–636
18) Wang K, Ho SY, Gibson DG, Anderson RH: Architecture of atrial musculature in humans. Br Heart J 1995; 73: 559–565
19) Nakagawa H, Lazzara R, Khastgir T, Beckman KJ, McClelland JH, Imai S, Pitha JV, Becker AE, Arruda M, Gonzales MD, Widman LE, Neuhauser J, Wang X, Calame JD, Goudeau MD, Jackman WM: Role of the tricuspid annulus and the Eustachian valve/ridge on atrial flutter: Relevance to catheter ablation of the septal isthmus and a new technique for rapid identification of ablation success. Circulation 1996; 94: 407–424

Circ J 2006; **70:** 321–326

Carvedilol Inhibits Mitochondrial Oxygen Consumption and Superoxide Production During Calcium Overload in Isolated Heart Mitochondria

Ryosuke Kametani, MD; Toshiro Miura, MD; Nozomu Harada, MD; Masaki Shibuya, MD; Ruijuan Wang, MD; Hong Tan, MD; Yasuhiro Fukagawa, MD; Shuji Kawamura, MD; Masunori Matsuzaki, MD

Background The COMET study suggested the better effect of carvedilol to metoprolol in treating heart failure. However, its underlying mechanisms of action remain unclear. As a result, evaluation of the distinct effects of both drugs on the mitochondrial function and reactive oxygen species (ROS) production during Ca^{2+} overload was investigated.

Methods and Results The mitochondrial oxygen consumption ($m\dot{V}O_2$) and the mitochondrial ROS production in isolated rat heart mitochondria was measured. Ca^{2+} overload from 10 to 100 μmol/L augmented $m\dot{V}O_2$ was from 527±139 to 671±138 nmol/mg ($p<0.05$), and this was then completely suppressed by carvedilol (1 μmol/L), but not by metoprolol (100 μmol/L). Ca^{2+} overload augmented the ROS production upon complex I injury (9.7±1.2 to 11.4±1.4 nmol/mg, $p<0.05$). Carvedilol dose-dependently suppressed this ROS production, whereas metoprolol did not.

Conclusions Carvedilol, but not metoprolol, was thus found to inhibit the calcium-dependent augmentation of $m\dot{V}O_2$ and ROS production upon complex I injury. This new effect of carvedilol might partly explain the beneficial effect of carvedilol for the treatment of heart failure. (*Circ J* 2006; **70:** 321–326)

Key Words: Calcium overload; Carvedilol; Mitochondria; Oxygen consumption; Superoxide

In the failing myocardium, calcium overload has been shown to play an important role in causing a dysfunction in the myocardium[1] and the reactive oxygen species (ROS) are produced from impaired mitochondria, which thus further impairs the cellular function[2–4] Beta-adrenergic receptor blockers have been shown to be effective for interrupting this malignant cycle of heart failure, thus attenuating both the calcium overload and the mitochondrial dysfunction[5,6] However, a recent clinical study, COMET, suggested that carvedilol had a better effect on the survival rate in patients with chronic heart failure than metoprolol[7] This study proposed that β2-adrenergic blocking, α-adrenergic receptor blocking, and other antioxidant effects might play a role in this occurrence. However, the underlying mechanism has yet to be well clarified. We hypothesized that carvedilol directly modifies the mitochondrial function, whereas also inhibiting the mitochondrial ROS production, especially from complex I[8] by α-, β-adrenergic receptor-independent mechanisms. To test this hypothesis, we isolated the rat heart mitochondria and evaluated the direct effect of carvedilol and metoprolol on the mitochondrial function, regarding such factors as the oxygen consumption and ROS production during calcium overload.

(Received November 14, 2005; revised manuscript received December 12, 2005; accepted December 16, 2005)

The Department of Cardiovascular Medicine, Yamaguchi University Graduate School of Medicine, Ube, Japan

Mailing address: Toshiro Miura, MD, The Department of Cardiovascular Medicine, Yamaguchi University Graduate School of Medicine, 1-1-1 Minami Kogushi, Ube 755-8505, Japan. E-mail: toshiro@yamaguchi-u.ac.jp

Methods

Animals

Male Sprague–Dawley rats (7–9 weeks old, 300–350 g) were anesthetized with the intra-peritoneal injection of sodium pentobarbital (60 mg/kg) and then the heart was excised and rinsed with an ice-cold buffer containing 300 mmol/L mannitol, 10 mmol/L HEPES, 0.2 mmol/L EDTA, and 0.1% bovine serum albumin (BSA). The pH was adjusted to 7.4 with KOH. The hearts were trimmed and homogenized with a motor-driven Teflon Potter homogenizer for 1 min in an ice-cold buffer.

Isolation of Heart Mitochondria

Mitochondria were then isolated by the centrifuge method, as previously described with slight modifications[9,10] The heart homogenate was centrifuged at 700 G for 10 min at 4°C using the KUBOTA 3780 centrifuge. The supernatant was decanted and centrifuged at 5,000 G for 8 min, followed by 10,000 G for 5 min. The pellet was resuspended using a paint brush and then it was centrifuged at 2,500 G for 10 min, followed by 9,000 G for 10 min. EDTA was omitted from the final washing buffer. The mitochondrial protein concentration was determined by the Bradford method using BSA as a standard. The mitochondrial suspension (4 mg/ml) was kept on ice until the measurements were performed, which were carried out after a 20-min recovery. All experiments conformed to the Guide for the Care and Use of Laboratory Animals (NIH Publication No.85-23) and the protocol was approved by the Animal Research Committee of Yamaguchi University, School of Medicine.

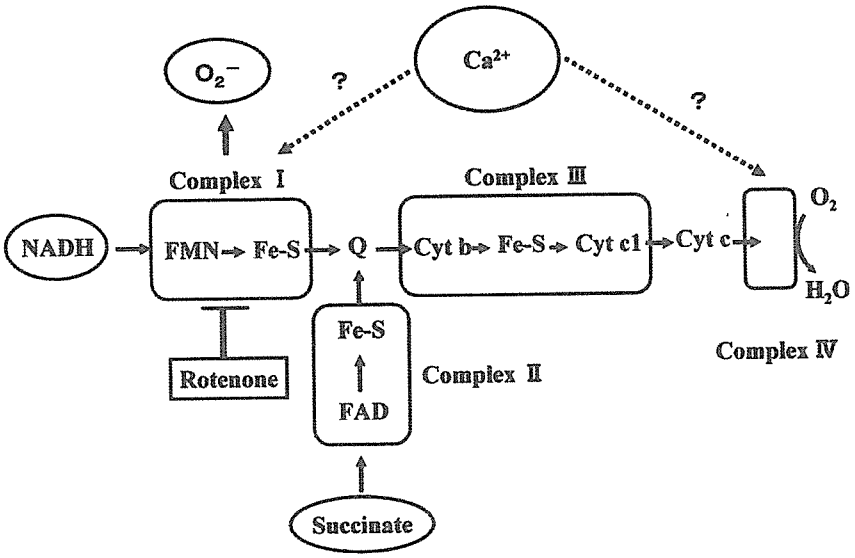

Fig 1. A schematic drawing of the components of the respiratory chain in mitochondria and the source of superoxide production. Rotenone inhibits complex I and the possible influence of Ca^{2+} overload is thus indicated. FAD, flavin adenine nucleotide; FMN, flavin mononucleotide; Fe-S, iron-sulfur protein; Q, ubiquinone; Cyt, cytochrome.

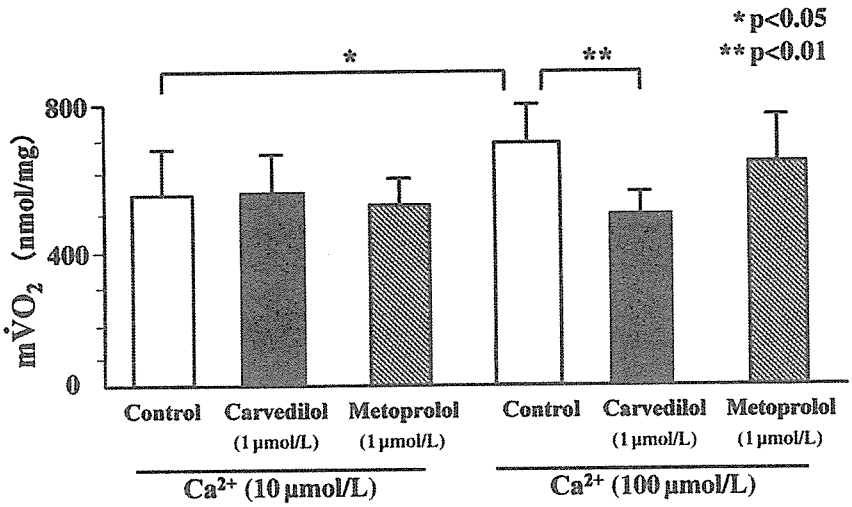

Fig 2. Mitochondrial O_2 consumption ($m\dot{V}O_2$) was significantly augmented by increasing Ca^{2+} from 10 to 100 μmol/L. Carvedilol (1 μmol/L) significantly suppressed the augmentation, whereas metoprolol did not. The data are expressed as the means ± SE, n=8 for each group.

Carvedilol was a gift from Daiichi Pharmaceutical (Tokyo, Japan) and it was dissolved in dimethyl sulfoxide (DMSO). The final concentration of DMSO was less than 0.1% when used. Metoprolol was purchased from Sigma and it was dissolved in normal saline.

Measurement of Mitochondrial Oxygen Consumption ($m\dot{V}O_2$)

$m\dot{V}O_2$ was measured using a Clark-type electrode (Instech Laboratories, Plymouth Meeting, PA, USA) in a 600-μl sealed glass chamber with water-jacketed and maintained at 37°C, with constant magnetic stirring. The oxygen tension in the chamber was monitored by the electrode connected to PowerLab Systems (ADInstruments, Colorado Springs, CO, USA). Mitochondria at a concentration of 0.2 mg/ml were incubated in the chamber with a medium consisting of 50 mmol/L HEPES. The reactions were initiated by adding NADH to a final concentration of 4 mmol/L. Carvedilol or metoprolol was added to the reaction medium before adding NADH. At 2 min after NADH was added, $CaCl_2$ was added to increase the calcium concentrations from 10 μmol/L to 100 μmol/L. The oxygen uptake was calibrated according to the oxygen consumed by mitochondria after addition of titrated solutions of NADH[11,12]

Measurement of ROS Production From Mitochondria

Two segments of the respiratory chain are primarily responsible for producing ROS in the mitochondria: namely NADH-ubiquinone reductase in complex I and biquinol-cytochorome *c* reductase in complex III (Fig 1)[13,14] ROS production was measured by lipid peroxidation, which was indicated by the amount of thiobarbituric acid reactive substance (TBARS)[15] The mitochondrial suspension (0.2 mg/ml) was incubated at 37°C in 600 μl HEPES buffer. Then either carvedilol or metoprolol was added 3 min before measuring the lipid peroxidation, which was initiated by the addition of NADH (4 mmol/L). $CaCl_2$ (10, 100 μmol/L), rotenone (100 μmol/L), and ADP/$FeSO_4$ (2 mmol/L/0.2 mmol/L) were added just before initiating lipid peroxidation. After 15 min, the samples were taken and mixed with 1.9 ml of TBARS reagent (0.75% thiobarbituric acid, 5 mol/L HCl, 10 mmol/L butylated hydroxytoluene). The mixture was heated at 80°C for 15 min, and then was cooled on ice for 10 min before centrifugation (400 G, 10 min). Lipid peroxidation was estimated by the appearance of TBARS with spectrophotometry quantified at 535 nm. The amount of TBARS was calculated using a molar extinction coefficient of 1.56×10^5 $(mol/L)^{-1}$ cm^{-1} and then it was expressed as nano moles of malondialdehyde

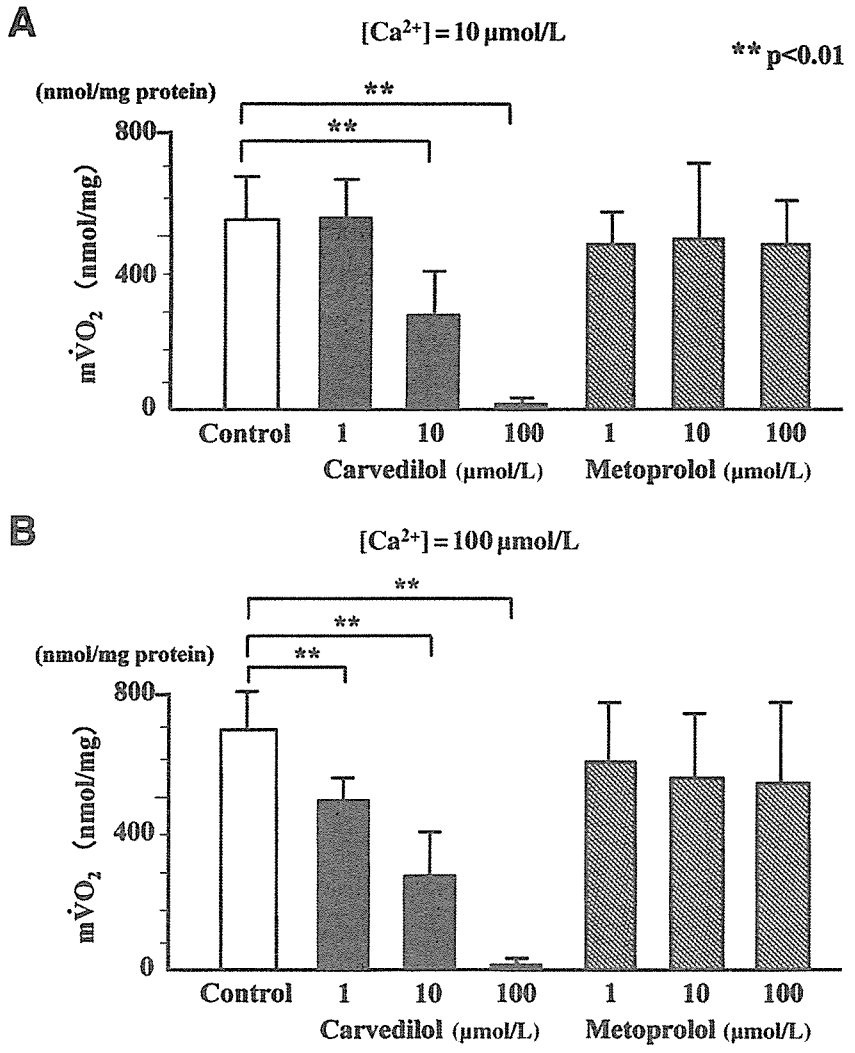

Fig 3. The dose-response effect of carvedilol and metoprolol on mitochondrial O_2 consumption during Ca^{2+} overload (3A: 10 μmol/L, 3B: 100 μmol/L). The data are expressed as the means ± SE, n=8 for each group. $m\dot{V}O_2$, mitochondrial O_2 consumption.

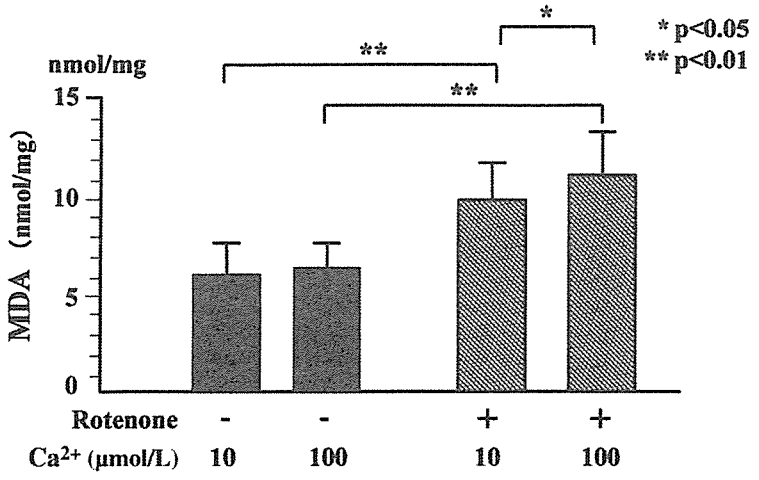

Fig 4. The effect of rotenone (100 μmol/L) on the malondialdehyde (MDA) production during Ca^{2+} overload ranging from 10 to 100 μmol/L. The data are expressed as the means ± SE, n=8 for each group.

(MDA) per mg of protein.[15]

Statistics

The data are expressed as the means ± SE. A statistical analysis was performed using one-way ANOVA followed by the multiple comparison Scheffe test. Differences with a value of $p < 0.05$ were considered to be significant.

Results

Mitochondrial O_2 Consumption

Fig 2 showed $m\dot{V}O_2$ 15 min after the addition of NADH. The $m\dot{V}O_2$ level significantly increased after adding Ca^{2+} to increase it from 10 to 100 μmol/L ($p<0.05$). A low dose of carvedilol (1 μmol/L) significantly reduced the augmented

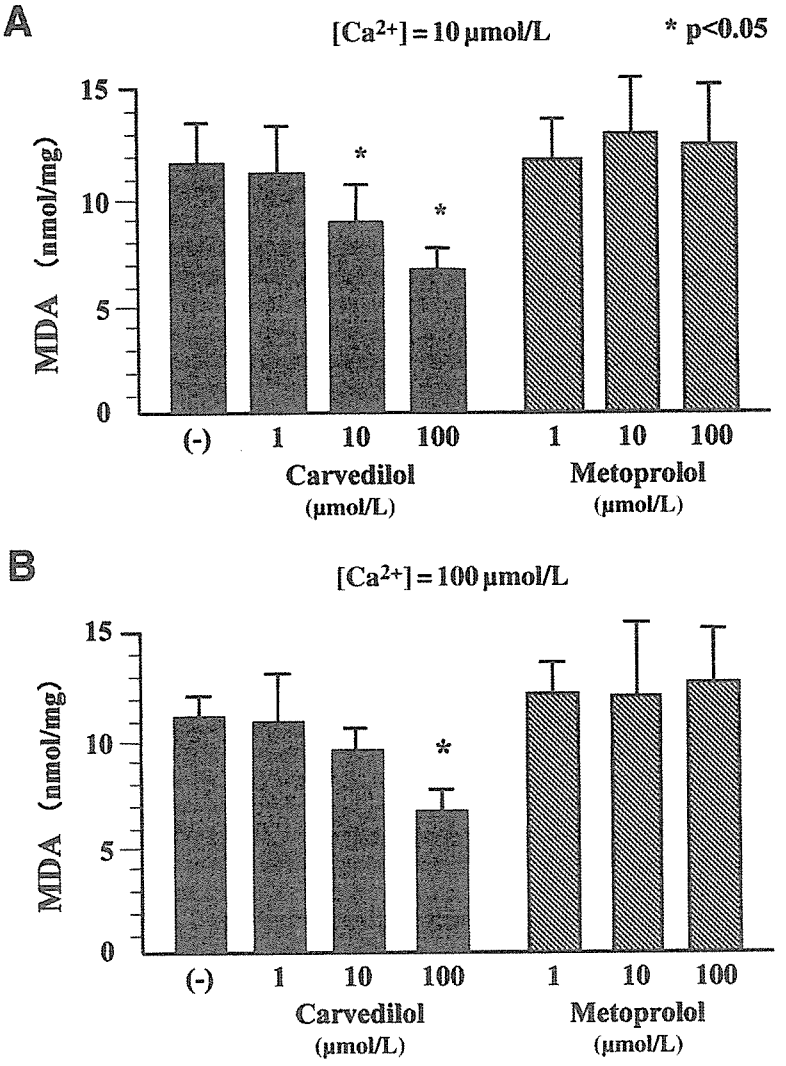

Fig 5. The dose-dependent effect of carvedilol and metoprolol on the production of mitochondrial ROS indicated by MDA amount under Ca^{2+} overload (5A: 10 μmol/L, 5B: 100 μmol/L). Carvedilol dose-dependently decreased the amount of ROS production, whereas metoprolol did not, even at high doses (100 μmol/L). ROS, reactive oxygen species; MDA, malondialdehyde. The data are expressed as the means ± SE, n=8 for each group.

$m\dot{V}O_2$ under Ca^{2+} overload (100 μmol/L). However, metoprolol (1 μmol/L) did not suppress the $m\dot{V}O_2$ during Ca^{2+} overload. Fig 3A shows the dose-response effect of carvedilol and metoprolol on $m\dot{V}O_2$ under calcium overload (10 μmol/L). Carvedilol dose-dependently reduced $m\dot{V}O_2$, but even 100 μmol/L metoprolol did not affect the $m\dot{V}O_2$ level. Fig 3B shows the effect of carvedilol and metoprolol on $m\dot{V}O_2$ under high Ca^{2+} overload (100 μmol/L). Even under a high Ca^{2+} overload, carvedilol dose-dependently reduced $m\dot{V}O_2$, however even higher doses of metoprolol (100 μmol/L) did not affect the $m\dot{V}O_2$ level.

Mitochondrial ROS Production During Ca^{2+} Overload

Fig 4 shows the amount of MDA produced 15 min after the addition of NADH to the mitochondria. Without rotenone (100 μmol/L), the Ca^{2+} overload ranging from 10 to 100 μmol/L did not affect the MDA production. However, the MDA production increased significantly with rotenone, and a Ca^{2+} overload ranging from 10 to 100 μmol/L then further increased the MDA production from the mitochondria. Fig 5 shows the effect of carvedilol and metoprolol on the MDA production at doses ranging from 10 μmol/L (Fig 5A) to 100 μmol/L (Fig 5B) of Ca^{2+} overload outside the mitochondria. Carvedilol dose-dependently decreased ROS production under the Ca^{2+} overload at both 10 and 100 μmol/L. However, even higher doses of metoprolol (100 μmol/L) did not affect the ROS production under Ca^{2+} overload.

Discussion

The present study showed for the first time that carvedilol, but not metoprolol, inhibited the augmentation of $m\dot{V}O_2$ caused by Ca^{2+} overload. Metabolic energy homeostasis is known to be maintained during changes in the cardiac workload, whereas Ca^{2+} plays an important role in mediating the signals for mitochondria to produce the required amount of adenosine triphosphate (ATP) needed to match the cardiac energy metabolism.[16] The proper coupling between the ATP requirement of the cardiomyocytes and the ATP production by the mitochondria is supposed to be regulated by the Ca^{2+} entry from the cytosol to the mitochondria,[17] but the precise mechanism which regulates the ATP production in the cardiac mitochondria according to the increased cellular demand remains unclear. In the present study, the Ca^{2+} outside of the mitochondria varied from 10 to 100 μmol/L in order to examine the direct effect of Ca^{2+} overload on the $m\dot{V}O_2$. We showed that the $m\dot{V}O_2$ was augmented by increasing the Ca^{2+} concentration outside the mitochondria. The increase in the $m\dot{V}O_2$ caused by

the Ca^{2+} overload can be explained by the following 2 mechanisms: one is the augmentation of the electron transport system by Ca^{2+} entry into the mitochondria, which thus leads to the enhanced production of ATP. This is supported by evidence that Ca^{2+} activates the F_0/F_1 ATPase activity, which synthesizes ATP in the cardiac mitochondria[18,19] The other mechanism is related to the uncoupling of the electron transport system, which did not increase ATP production[20] This uncoupling is characterized by the proton leak through the mitochondrial inner membrane, which results in the disruption of the H^+ gradient formed across the inner mitochondrial membrane by the electron transport system. When the uncoupling phenomenon occurs because of the calcium overload[21] despite of any increase in the oxygen consumption, the ATP synthesis did not increase accordingly[22]

Effect of Carvedilol on Ca^{2+} Dependent $m\dot{V}O_2$

Our result suggests that carvedilol suppresses $m\dot{V}O_2$ directly without any signaling from the β-adrenergic receptor system. The downstream cascade of β-adrenergic receptor stimulation includes cAMP, protein kinase A, and several phosphorylated proteins including the L-type calcium channels, phospholamban, and ryanodine receptors[23] However, the signaling to the mitochondria from the β-adrenergic receptor pathway has not yet been well elucidated. The cytosolic Ca^{2+} most likely plays an important role in mediating the β-adrenergic receptor signals to the mitochondria in order to regulate the ATP production[24] As a result, carvedilol might act to inhibit the Ca^{2+} entry into the mitochondria. Carvedilol can also inhibit the augmented $m\dot{V}O_2$ caused by Ca^{2+} overload through an inhibitory effect on the respiratory uncoupling. In addition, the protonophoretic characterisctics of carvedilol might be involved in this mechanism[25] Because the direct effect of carvedilol on the mitochondria was examined in the present study, isolated mitochondrial experiments were thus carried out. Although the effect of antioxidant and anti-apoptotic effect on the in vitro isolated cardiomyocyte has been shown[26,27] the direct effect of carvedilol on mitochondria during calcium overload has never been evaluated. The impact of the present study on the treatment of heart failure thus needs to be further clarified. By either mechanism, carvedilol was found to have a direct effect on the mitochondria thus resulting in the inhibition of the oxygen consumption during Ca^{2+} overload independent of the β-adrenergic system[28]

Mechanism of Augmented ROS Production by Ca^{2+} and Rotenone

The present study found that the normal mitochondria isolated from the rat cardiomyocytes did not increase the ROS production as measured by the amount of MDA under Ca^{2+} overload. However, the mitochondria mimicking a state of heart failure by impairing complex I with rotenone (100 μmol/L) became sensitive to Ca^{2+} overload in order to increase the ROS production. This occurrence has also been observed for the forebrain mitochondria, but not for the isolated mitochondria from either liver or skeletal muscle[29] Rotenone was used as an inhibitor of complex I in a mitochondrial electron transport system, which is known to be impaired in a state of heart failure (Fig 1). In a state of heart failure, complex I has been shown to be a major source of ROS in the mitochondria[8] and this rotenone specific domain has also been shown to be sensitive to Ca^{2+} in the production of ROS[29] As a result, carvedilol might act on this rotenone-sensitive domain of complex I in order to inhibit the ROS production caused by Ca^{2+} overload. In addition, these mechanisms can also be specific for the heart and forbrain, but not for the liver or skeletal muscle[29]

Distinct Effects Between Carvedilol and Metoprolol

We herein showed that the effect of carvedilol on the mitochondrial function, such as oxygen consumption and ROS production, is distinct from that of metoprolol. Both carvedilol and metoprolol are known to be potent β-adrenergic receptor blockers, which can thus suppress Ca^{2+} overload by stabilizing the calcium release channels (ryanodine receptors) on the sarcoplasmic reticulum[23] and clinical trials of both drugs have shown these drugs to be effective in treating chronic heart failure[30] However, a recent study comparing the effect of carvedilol and metoprolol, called the COMET study[7] indicated carvedilol to have a better efficacy in comparison to metoprolol regarding the event-free survival in heart failure patients. The present study further provides definite evidence that carvedilol differs significantly from metoprolol in inhibiting the Ca^{2+} overload-induced mitochondrial oxygen consumption and the ROS production during an impairment of complex I. Previous studies also support our results using different models[26,31] This distinct effect between the drugs might partly explain the results of the COMET study, ie, a β_1-adrenergic receptor independent effect[27] Importantly, carvedilol suppressed the production of ROS, especially during an impairment of complex I, which mimics a state of heart failure[8] The ROS production has been shown to be enhanced in a state of heart failure because of the β_1-adrenoceptor dependent pathway[32] As a result, it is conceivable that the β_1-adrenoceptor blockades reduced the ROS production through the β_1-adrenoceptor pathway[33] However, ROS could be produced by many different pathways such as the angiotensin II mediated pathways through the activation of NADPH oxidase and the TNF mediated pathways in patients with heart failure[34,35] The antioxidant effect of carvedilol might inhibit all ROS-induced toxic effect on both intracellular and mitochondrial calcium handling, because this effect is independent of the β-adrenoceptor pathway. Therefore, carvedilol might be more effective during the state of heart failure than under normal conditions[36] Finally, the rationale regarding the dose used in the present study needs to be discussed. The ID_{50} for β_1-adrenoceptors might be lower in carvedilol than in metoprolol, but the ID_{50} for β_1-adrenoceptor blocking effect is nanomolar order for both drugs. As a result, the micromolar order of the concentration used in the present study is sufficient to block β_1-adrenoceptors by both drugs. Moreover, the antioxidant effect of the drugs might not necessarily coincide with the β_1-adrenoceptor blocking effect. Since the 100 μmol/L metoprolol did not show any effect in the present study, our conclusions will therefore not change regardless of the dose used.

Aknowledgemements

We thank Ms Kazuko Iwamoto and Rie Ishihara for their excellent technical assistance. The present study was partially supported by a Grant-in-Aid for Scientific Research from the Japan Society for the Promotion of Science, Japan (No.13670716 to T.M.) and a research grant from Daiichi Pharmaceutical Company.

References

1. Fleckenstein A. Myocardial fiber necrosis due to intracellular Ca overload-a new principle in cardiac pathophysiology. *Recent Adv Stud Cardiac Struct Metab* 1974; **4:** 563–580.
2. Ruffolo RR Jr, Feuerstein GZ. Neurohormonal activation, oxygen free radicals, and apoptosis in the pathogenesis of congestive heart failure. *J Cardiovasc Pharmacol* 1998; **32:** S22–S30.
3. Ide T, Tsutsui H, Kinugawa S, Suematsu N, Hayashidani S, Ichikawa K, et al. Direct evidence for increased hydroxyl radicals originating from superoxide in the failing myocardium. *Circ Res* 2000; **86:** 152–157.
4. Ishikawa K, Kimura S, Kobayashi A, Sato T, Matsumoto H, Ujiie Y, et al. Increased reactive oxygen species and anti-oxidative response in mitochondrial cardiomyopathy. *Circ J* 2005; **69:** 617–620.
5. Reiken S, Wehrens XH, Vest JA, Barbone A, Klotz S, Mancini D, et al. Beta-blockers restore calcium release channel function and improve cardiac muscle performance in human heart failure. *Circulation* 2003; **107:** 2459–2466.
6. Stanley WC, Hoppel CL. Mitochondrial dysfunction in heart failure: Potential for therapeutic interventions? *Cardiovasc Res* 2000; **45:** 805–806.
7. Poole-Wilson PA, Swedberg K, Cleland JG, Di Lenard A, Hanrath P, Komajda M, et al. Comparison of carvedilol and metoprolol on clinical outcomes in patients with chronic heart failure in the carvedilol or metoprolol European trial (COMET): Randomised controlled trial. *Lancet* 2003; **362:** 7–13.
8. Ide T, Tsutsui H, Kinugawa S, Utsumi H, Kang D, Hattori N, et al. Mitochondrial electron transport complex I is a potential source of oxygen free radicals in the failing myocardium. *Circ Res* 1999; **85:** 357–363.
9. Green DE, Kohout PM. Isolation of succinic dehydrogenase from beef heart mitochondria. *Biochim Biophys Acta* 1954; **14:** 295–296.
10. La Noue KF, Duszynski J, Watts JA, McKee E. Kinetic properties of aspartate transport in rat heart mitochondrial inner membranes. *Arch Biochem Biophys* 1979; **95:** 578–590.
11. Chance B, Hagihara B. Initiation of succinate oxidation in aged pigeon heart mitochondria. *Biochem Biophys Res Commun* 1960; **8:** 180–185.
12. Estabrook RW. Mitochondrial respiratory control and the polarographic measurement of ADP: O ratios. *Methods Enzymol* 1967; **10:** 41–47.
13. Turrens JF. Generation of superoxide anion by the NADH dehydrogenase of bovine heart mitochondria. *Biochem J* 1980; **191:** 421–427.
14. Turrens JF. Ubisemiquinone is the electron donor for superoxide formation by complex III of heart mitochondria. *Arch Biochem Biophys* 1985; **237:** 408–414.
15. Buege JA, Aust SD. Microsomal lipid peroxidation. *Methods Enzymol* 1978; **52:** 302–310.
16. Saks VA, Kuznetsov AV, Vendelin M, Guerrero K, Kay L, Seppet EK. Functional coupling as a basic mechanism of feedback regulation of cardiac energy metabolism. *Mol Cell Biochem* 2004; **256:** 185–199.
17. McCormack JG, Halestrap AP, Denton RM. Role of calcium ions in regulation of mammalian intramitochondrial metabolism. *Physiol Rev* 1990; **70:** 391–425.
18. Jouaville LS, Pinton P, Bastianutto C, Rutter GA, Rizzuto R. Regulation of mitochondrial ATP synthesis by calcium: Evidence for a long-term metabolic priming. *Proc Natl Acad Sci USA* 1999; **96:** 13807–13812.
19. Territo PR, Mootha VK, French SA, Balaban RS. Ca^{2+} activation of heart mitochondrial oxidative phosphorylation: Role of the F_0/F_1-ATPase. *Am J Physiol Cell Physiol* 2000; **278:** C423–C435.
20. Sentex E, Laurent A, Martine L, Gregoire S, Rochette L, Demaison L. Calcium- and ADP-magnesium-induced respiratory uncoupling in isolated cardiac mitochondria: Influence of cyclosporin A. *Mol Cell Biochem* 1999; **202:** 73–84.
21. Meynier A, Razik H, Cordelet C, Gregoire S, Demaison L. Involvement of oxygen free radicals in the respiratory uncoupling induced by free calcium and ADP-magnesium in isolated cardiac mitochondria: Comparing reoxygenation in cultured cardiomyocytes. *Mol Cell Biochem* 2003; **243:** 55–64.
22. Kingsley-Hickman PB, Sako EY, Ugurbil K, From AH, Foker EJ. ^{31}P NMR measurement of mitochondrial uncoupling in isolated rat hearts. *J Biol Chem* 1990; **265:** 1545–1550.
23. Marx SO, Reiken S, Hisamatsu Y, Jayaraman T, Burkhoff D, Rosemblit N, et al. PKA phosphorylation dissociates FKBP12.6 from the calcium release channel (ryanodine receptor): Defective regulation in failing hearts. *Cell* 2000; **101:** 365–376.
24. Hayakawa Y, Nemoto T, Iino M, Kasai H. Rapid Ca^{2+}-dependent increase in oxygen consumption by mitochondria in single mammalian central neurons. *Cell Calcium* 205; **37:** 359–370.
25. Oliveira PJ, Marques MP, Batista de Carvalho LA, Moreno AJ. Effects of carvedilol on isolated heart mitochondria: Evidence for a protonophoretic mechanism. *Biochem Biophys Res Commun* 2000; **276:** 82–87.
26. Lysko PG, Webb CL, Gu JL, Ohlstein EH, Ruffolo RR Jr, Yue TL. A comparison of carvedilol and metoprolol antioxidant activities in vitro. *J Cardiovasc Pharmacol* 2000; **36:** 277–281.
27. Schwarz ER, Kersting PH, Reffelmann T, Meven DA, Al-Dashti R, Skobel EC, et al. Cardioprotection by Carvedilol: Antiapoptosis is independent of beta-adrenoceptor blockage in the rat heart. *J Cardiovasc Pharmacol Ther* 2003; **8:** 207–215.
28. Yao A, Kohmoto O, Oyama T, Sugishita Y, Shimizu T, Harada K, et al. Characteristic effects of alpha1-beta1,2-adrenergic blocking agent, carvedilol, on $[Ca^{2+}]_i$ in ventricular myocytes compared with those of timolol and atenolol. *Circ J* 2003; **67:** 83–90.
29. Sousa SC, Maciel EN, Vercesi AE, Castilho RF. Ca^{2+}-induced oxidative stress in brain mitochondria treated with the respiratory chain inhibitor rotenone. *FEBS Lett* 2003; **543:** 179–183.
30. Domanski MJ, Krause-Steinrauf H, Massie BM, Deedwania P, Follmann D, Kovar D, et al. A comparative analysis of the results from 4 trials of beta-blocker therapy for heart failure: BEST, CIBIS-II, MERIT-HF, and COPERNICUS. *J Card Fail* 2003; **9:** 354–363.
31. Arumanayagam M, Chan S, Tong S, Sanderson JE. Antioxidant properties of carvedilol and metoprolol in heart failure: A double-blind randomized controlled trial. *J Cardiovasc Pharmacol* 2001; **37:** 48–54.
32. Nishizawa T, Iwase M, Kanazawa H, Ichihara S, Ichihara G, Nagata K, et al. Serial alterations of β-adrenergic signaling in dilated cardiomyopathic hamsters: Possible role of myocardial oxidative stress. *Circ J* 2004; **68:** 1051–1060.
33. Kukin ML, Kalman J, Charney RH, Levy DK, Buchholz-Varley C, Ocampo ON, et al. Prospective, randomized comparison of effect of long-term treatment with metoprolol or carvedilol on symptoms, exercise, ejection fraction, and oxidative stress in heart failure. *Circulation* 1999; **99:** 2645–2651.
34. Keith M, Geranmayegan A, Sole MJ, Kurian R, Robinson A, Omran AS, et al. Increased oxidative stress in patients with congestive heart failure. *J Am Coll Cardiol* 1998; **31:** 1352–1356.
35. Sorescu D, Griendling KK. Reactive oxygen species, mitochondria, and NAD(P)H oxidases in the development and progression of heart failure. *Congest Heart Fail* 2002; **8:** 132–140.
36. Nakamura K, Kusano K, Nakamura Y, Kakishita M, Ohta K, Nagase S, et al. Carvedilol decreases elevated oxidative stress in human failing myocardium. *Circulation* 2002; **105:** 2867–2871.

Original Article

Different Effects of Amlodipine and Enalapril on the Mitogen-Activated Protein Kinase/Extracellular Signal-Regulated Kinase Kinase–Extracellular Signal-Regulated Kinase Pathway for Induction of Vascular Smooth Muscle Cell Differentiation *In Vivo*

Seiji UMEMOTO[1], Shinji KAWAHARA[2], Ryo HASHIMOTO[2], Kyoko UMEJI[2], Susumu MATSUDA[2], Masakazu TANAKA[2], Makoto KUBO[2], and Masunori MATSUZAKI[2]

Although recent clinical trials have shown that amlodipine exerts antiatherogenic effects, the mechanism of these effects remains unknown. This study was designed to examine which signal transduction pathway might be important for the antiatherogenic property of amlodipine, as assessed by aortic smooth muscle cell (SMC) phenotypes in hypertension *in vivo*. Stroke-prone spontaneously hypertensive rats (SHRSP) were randomly treated with a vehicle, amlodipine, or enalapril while Wistar-Kyoto rats (WKY) used as controls were treated with only the vehicle. Both drugs were equally effective at reducing systolic blood pressure, and inhibiting the progression of aortic remodeling and fibrosis in comparison to those of vehicle-treated SHRSP. In the aortas of vehicle-treated SHRSP, the level of contractile-type smooth muscle (SM) myosin heavy chain (MHC) SM2 was significantly lower, whereas the level of synthetic-type MHC NMHC-B/SMemb was significantly higher compared with those in the WKY aortas. Compared to the vehicle-treated SHRSP group, both drugs significantly and equally shifted the aortic SMC phenotype in SHRSP toward the differentiated state by reducing NMHC-B/SMemb and increasing SM2. The levels of MKK6, p38 MAPK, MEK1 and p-42/44 ERK were significantly higher in the vehicle-treated SHRSP than in the WKY. Both drugs significantly reduced these values in the SHRSP aorta. Furthermore, the levels of MEK1 and p-42/44 ERK were significantly lower in the amlodipine- than in the enalapril-treated SHRSP group, whereas enalapril was more effective than amlodipine at increasing p-Akt and endothelial NO synthase in SHRSP aortas, which were significantly lower in the vehicle SHRSP group than in the WKY group. Thus, the MEK-ERK pathway might be one of the crucial determinants of the aortic SMC phenotype activated by amlodipine treatment of hypertension *in vivo*. (*Hypertens Res* 2006; 29: 179–186)

Key Words: **hypertension, calcium antagonist, signal transduction, smooth muscle cell**

From the [1]Pharmaceutical Clinical Research Center, Yamaguchi University Hospital, Ube, Japan; and [2]Department of Cardiovascular Medicine, Yamaguchi University Graduate School of Medicine, Ube, Japan.

This study was supported in part by grants from Eisai Co., Ltd., Sumitomo Pharmaceuticals, and the Takeda Science Foundation.

Address for Reprints: Seiji Umemoto, M.D., Ph.D., Pharmacological Clinical Research Center, Yamaguchi University Hospital, 1-1-1 Minami-Kogushi, Ube 755-8505, Japan. E-mail: umemoto@yamaguchi-u.ac.jp

Received August 5, 2005; Accepted in revised form December 26, 2005.

Introduction

Vascular smooth muscle cells (SMCs) exist in a diverse range of phenotypes, and the phenotypic modulation of vascular SMCs is a hallmark of vascular dysfunction in hypertension (*1*, *2*). Under physiologic conditions, vascular SMCs exhibit the differentiated/contractile phenotype, whereas, under pathologic conditions, vascular SMCs display a proliferative/dedifferentiated phenotype and are involved in the progression of atherosclerosis (*1*). SMCs in the media express 2 isoforms of the smooth muscle (SM) myosin heavy chain (MHC; SM1 and SM2) and 2 types of nonmuscle MHC (NMHC) isoforms (NMHC-B/SMemb and NMHC-A) (*1*, *2*). We recently reported that angiotensin II receptor type 1–mediated NAD(P)H oxidase–generated reactive oxygen species, endothelial NO synthase (eNOS) and phosphoinositide 3-kinase (PI3-K)/protein kinase B (PKB) (Akt), as well as GATA-6, a zinc finger transcription factor that regulates SM-MHC isoforms in vascular SMCs, might be crucial determinants for the vascular SMC phenotype in hypertension *in vivo* (*3*, *4*). It has also been reported that the forced expression of active forms of mitogen-activated protein (MAP) kinase/extracellular signal-regulated kinase (ERK) kinase (MEK) 1 and MAP kinase (MAPK) kinase (MKK) 6, which are the upstream kinases of ERK and p38 MAPK, respectively, induced de-differentiation of SMCs, indicating that the SMC phenotype would be determined by the balance between the strengths of the Akt pathway and the ERK and p38 MAPK pathways (*5*).

The calcium antagonists have been widely used in the treatment of patients with hypertension (*6–8*), in whom they inhibit cardiovascular events as effectively as angiotensin-converting enzyme (ACE) inhibitors (*7–9*). In addition, recent clinical studies have revealed that the long-acting L-type dihydropyridine calcium antagonist amlodipine may have antiatherogenic properties independent of its effects on vasodilatation (*10–12*). We have also shown that amlodipine may have antiatherosclerotic antioxidative action beyond blood-pressure lowering in stroke-prone spontaneously hypertensive rat (SHRSP) hearts (*13*). However, the precise mechanisms regulating vascular SMC phenotypic modulation and the critical signal transductions affecting the vascular SMC phenotype in hypertension by amlodipine remain unclear *in vivo*. The purpose of this study was to examine which signal transduction pathway(s) might be crucial to the antiatherogenic property of amlodipine, and regulate the aortic SMC phenotype in SHRSP *in vivo*.

Methods

Experimental Protocol

The Ethics Committee for Animal Experimentation at the Yamaguchi University School of Medicine approved the experimental protocol. The long-acting L-type dihydropyridine calcium antagonist amlodipine and the ACE inhibitor enalapril were provided by Pfizer Pharmaceuticals Inc. (Tokyo, Japan) and Banyu Pharmaceutical Co., Ltd. (Tokyo, Japan), respectively. Twelve-week-old male Wistar-Kyoto rats (WKY group; $n=20$) and SHRSP ($n=60$) were obtained from Charles River Japan (Yokohama, Japan). The WKY group was treated with a vehicle, and the SHRSP were randomly treated with a vehicle (SHRSP group), amlodipine (5 mg/kg per day, amlodipine group), or enalapril (10 mg/kg per day, enalapril group). The doses used in the experiments were determined according to Umemoto *et al.* (*13*). Without anesthetizing the rats, systolic blood pressure (SBP) and heart rate were obtained by tail-cuff plethysmography. After the 6-week treatment period, the rats were weighed, euthanized with a sodium pentobarbital overdose and perfusion-fixed for 5 min at a pressure of 90 mmHg with heparinized saline followed by Bouin's solution; then, paraffin slices (4-μm thick) of the thoracic aortas were stained with Sirius red as previously reported (*3*). Care was taken not to damage either the endothelium or the medial layer. The other rats were also euthanized by an intraperitoneal sodium pentobarbital overdose, and then the rat thoracic aortas were immediately rinsed with phosphate-buffered saline to remove adventitial fat and connective tissue by blunt dissection, frozen in liquid nitrogen, and stored at −80°C until used for immunoblots (*3*). In some experiments, the endothelium was denuded as previously reported (*3*).

Histological Analysis

The total cell number in the aortic tunica media, the wall thickness/lumen ratio (the medial thickness to the internal diameter), and the percentage of the total collagen volume fraction determined by Sirius red staining were measured from 5 randomly selected fields in 1 cross-section of the aorta in a blind fashion using a computer-assisted image analysis system as previously reported (*3*), and the mean value of each aorta was used for statistical analysis.

Immunoblotting

The following were applied for immunoblotting using the enhanced chemiluminescence (ECL™) system (Amersham Biosciences, Piscataway, USA) as previously reported (*3*): mouse monoclonal antibody against human α-SM actin (DakoCytomation, Kyoto, Japan), mouse monoclonal antibodies against rabbit contractile-type SM-MHC isoform SM2 and NMHC-B/SMemb (Yamasa, Choshi, Japan), and human eNOS (Transduction Laboratories, Lexington, USA), goat polyclonal antibodies against human Akt and MKK6, rabbit polyclonal antibody against mouse p38 MAPK and rat MEK1, mouse monoclonal antibodies against human phospho-42/44 ERK (p-42/44 ERK) and phospho-p38 MAPK (p-p38 MAPK) (Santa Cruz Biotech, Santa Cruz, USA), and rabbit polyclonal antibodies against rat 42/44 ERK and mouse

Table 1. Heart Rate, Body Weight, Wall-to-Lumen Ratio, Total Cell Number, and Collagen Volume Fraction in 18-Week-Old Rats

Parameter	WKY	SHRSP	Amlodipine	Enalapril
Heart rate (bpm)	306±13	330±13	309±14	288±9
Body weight (g)	409±16	315±9*	315±5*	320±5*
Wall-to-lumen ratio	0.05±0.004	0.086±0.002*	0.069±0.003†,§	0.067±0.004†,‡
Total cell number	2,046±181	2,474±126	2,326±106	2,054±89
Collagen volume fraction (%)	2.8±0.2	5.0±0.3*	3.9±0.2†,§	3.9±0.3†,§

Values are means±SEM. SHRSP were treated with vehicle, amlodipine (5 mg/kg per day), or enalapril (10 mg/kg per day) for 6 weeks. *$p<0.01$, †$p<0.05$ *vs.* the WKY group; ‡$p<0.01$, §$p<0.05$ *vs.* the vehicle SHRSP group. Experiments: $n=5$–6. WKY, Wistar-Kyoto rats; SHRSP, stroke-prone spontaneously hypertensive rats.

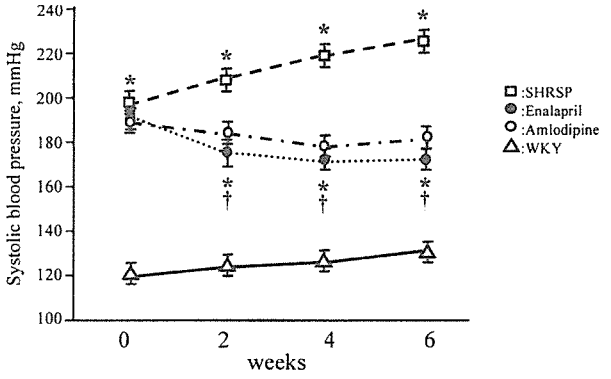

Fig. 1. *Graphs showing systolic blood pressure (SBP) in the vehicle SHRSP, amlodipine, and enalapril groups. Bars indicate SEM.* *p<*0.01* vs. *the WKY group,* †p<*0.01* vs. *the vehicle SHRSP group. Experiments,* n=*5–7.*

phospho-Akt (p-Akt) (Cell Signaling Technology, Beverly, USA). The ratios of each protein (SM2, NMHC-B/SMemb, eNOS, MKK6, and MEK1) to α-SM actin (as an internal standard), the ratio of p-Akt to total Akt, the ratio of p-p38 MAPK to total p38 MAPK, and the ratio of p-42/44 ERK to total 42/44 ERK were obtained by calculating the percentage of each protein expression *vs.* the vehicle WKY group, respectively.

Statistical Analysis

All values are expressed as the means±SEM. The experimental groups were compared by ANOVA followed by Scheffe's multiple comparisons. Values of $p<0.05$ were considered statistically significant.

Results

The heart rate was unaltered among the 4 groups (Table 1). Throughout the experiments, SBP in the vehicle SHRSP group was significantly higher than that in the WKY group. The two drugs significantly and equally reduced SBP compared with that in the vehicle SHRSP group. However, both the amlodipine and enalapril groups showed significantly higher SBP than the WKY group (Fig. 1). Body weight was greater in the WKY group than in the 3 SHRSP groups, but there was no difference in the body weights among the vehicle and the 2 drug-treated SHRSP groups (Table 1).

The wall-to-lumen ratio and collagen volume fraction were increased in the vehicle SHRSP group compared with the WKY group. The 2 drug-treated groups had significantly lower values than the vehicle SHRSP group. There were no significant differences in these values between the 2 drug-treated SHRSP groups, but the values were still significantly higher than in the WKY group. There was little difference in the total cell number in the aortic media among the 4 groups (Table 1).

Figure 2 shows that SM2 expression in the aorta was significantly decreased in the vehicle SHRSP group compared with the WKY group. Compared with the vehicle SHRSP group, SM2 expression in the aorta was significantly higher in both the amlodipine and enalapril groups, with no significant difference seen between the 2 drug-treated groups. However, the level of SM2 expression in both drug-treated groups was still significantly lower than that in the WKY group. In contrast, NMHC-B/SMemb expression in the aorta was significantly higher in the vehicle SHRSP group compared with the WKY group. Compared with the vehicle SHRSP group, NMHC-B/SMemb expression in the aorta was significantly lower in both the amlodipine and enalapril groups, with no significant difference seen between the 2 drug-treated groups. The level of NMHC-B/SMemb expression in both the drug-treated groups was, however, still significantly greater than that in the WKY group.

We further examined which signal transduction regulates the rat aortic SMC phenotype *in vivo*. The expressions of p-p38 MAPK and p-42/44 ERK in the aortas were significantly higher in the vehicle SHRSP group than in the WKY group (Fig. 3). The 2 drug-treated groups had significantly lower aortic expressions of both p-p38 MAPK and p-42/44 ERK than the vehicle SHRSP group. Both drugs reduced p-p38 MAPK in SHRSP aortas, with no significant difference seen between the 2 drug-treated groups, whereas amlodipine was

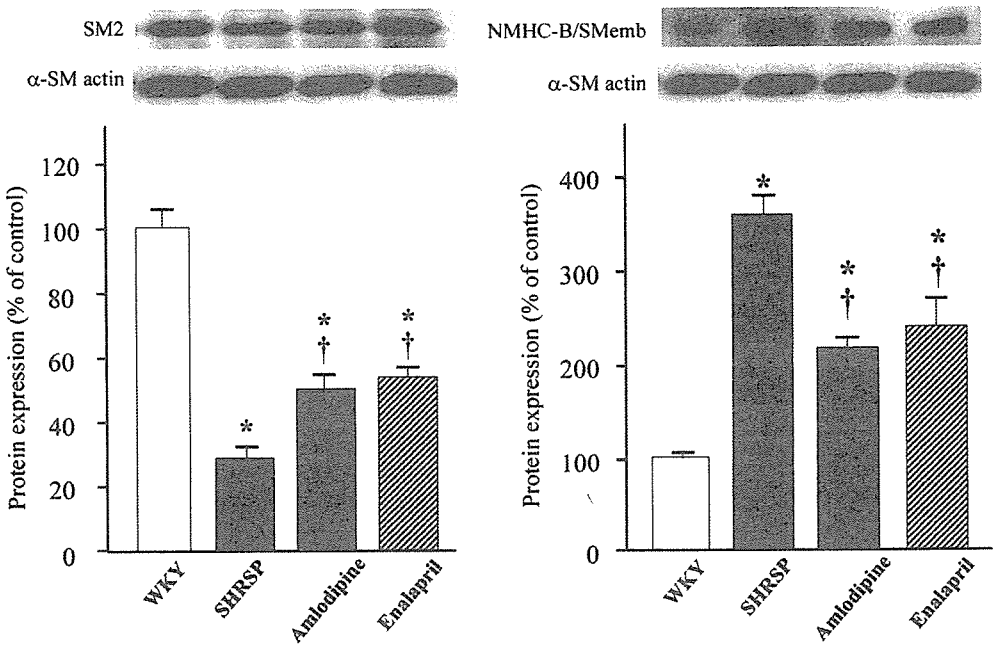

Fig. 2. *Quantitative analysis of SM2 and NMHC-B/SMemb expressions in the rat aortas. Bars indicate SEM.* *p<*0.01* vs. *the WKY group;* †p<*0.01* vs. *the vehicle SHRSP group. Experiments:* n=*6*.

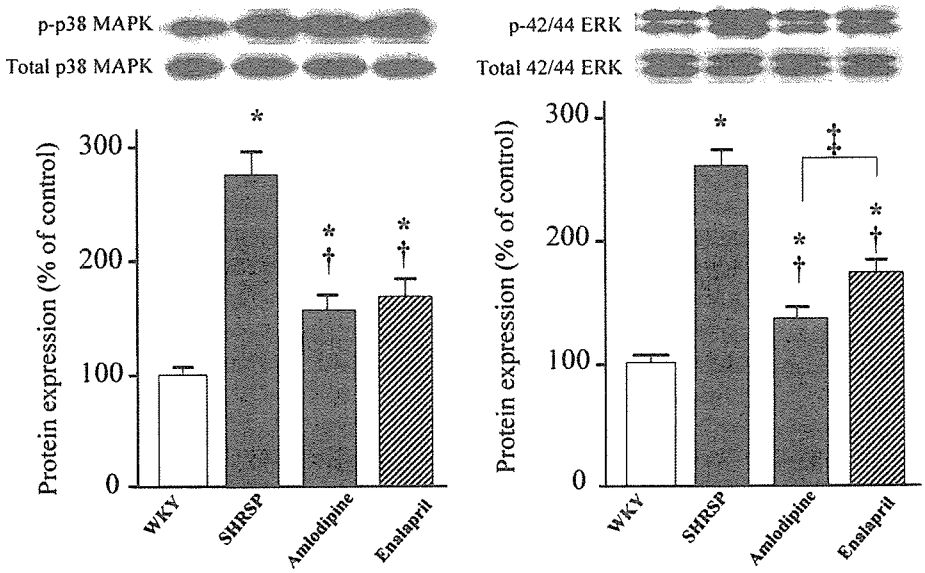

Fig. 3. *Quantitative analysis of p-p38 MAPK and p-42/44 ERK expression in the rat aortas. Bars indicate SEM.* *p<*0.05* vs. *the WKY group;* †p<*0.01* vs. *the vehicle SHRSP group;* ‡p<*0.05* vs. *the amlodipine group. Experiments:* n=*6*.

more effective than enalapril at decreasing p-42/44 ERK expression in SHRSP aortas. The level of p-p38 MAPK and p-42/44 ERK expressions in both the drug-treated groups was, however, still significantly greater than that in the WKY group.

We also examined the aortic expressions of MKK6 and MEK1, the upstream kinases of MAPK and ERK, respectively, which were significantly higher in the vehicle SHRSP group than in the WKY group (Fig. 4). The two drugs significantly reduced these values in SHRSP aortas. Both drugs reduced MKK6 in SHRSP aortas, with no significant difference seen between the 2 drug-treated groups, whereas amlodipine was more effective than enalapril at decreasing MEK1 expression in SHRSP aortas to the same level as in the WKY